nature structural & molecular biology

The Elongator subcomplex Elp456 is a hexameric RecA-like ATPase

Sebastian Glatt[1], Juliette Létoquart[2–4], Céline Faux[2–4], Nicholas M I Taylor[1], Bertrand Séraphin[2–4] & Christoph W Müller[1]

Elongator was initially described as an RNA polymerase II–associated factor but has since been associated with a broad range of cellular activities. It has also attracted clinical attention because of its role in certain neurodegenerative diseases. Here we describe the crystal structure of the *Saccharomyces cerevisiae* subcomplex of Elongator proteins 4, 5 and 6 (Elp456). The subunits each show almost identical RecA folds that form a heterohexameric ring-like structure resembling hexameric RecA-like ATPases. This structural finding is supported by different complementary *in vitro* and *in vivo* approaches, including the specific binding of the hexameric Elp456 subcomplex to tRNAs in a manner regulated by ATP. Our results support a role of Elongator in tRNA modification, explain the importance of each of the Elp4, Elp5 and Elp6 subunits for complex integrity and suggest a model for the overall architecture of the holo-Elongator complex.

The Elongator complex was first identified in yeast as a histone acetyltransferase (HAT) complex that associates with the hyperphosphorylated elongating form of RNA polymerase II (ref. 1). However, since its initial discovery, Elongator has been shown to be involved with a variety of different cellular functions, including histone acetylation[1], exocytosis[2], α-tubulin tail acetylation[3], sensitivity to DNA damaging agents and transcriptional silencing[4], zygotic paternal genome demethylation[5] and tRNA modification[6,7]. Among these respective biochemical activities, post-transcriptional tRNA modification activity has recently gained particular attention. Elongator has been reported to be involved in the generation of 5-methoxycarbonylmethyl (mcm^5) and 5-carbamoylmethyl (ncm^5) groups on uridine nucleosides present at the wobble position of eukaryotic tRNAs[8,9]. Modifications of the wobble position U of tRNAs have been reported to preorder the anticodon loop, thereby promoting favorable base stacking, which stabilizes codon-anticodon interaction in certain G3U34 wobble pairs[10,11]. The mcm^5 or ncm^5 modifications affect 11 of the 13 yeast tRNAs with U at the wobble position and thus might have a substantial impact on translation accuracy[10]. Of particular note, overexpression of two tRNA species in *S. cerevisiae* was sufficient to rescue phenotypes originally linked to proposed Elongator functions in transcription elongation and exocytosis[6], suggesting that loss of tRNA modification activity may account for several of the highly divergent phenotypes associated with the inactivation of Elongator.

The three Elongator proteins Elp1, Elp2 and Elp3 were the first Elongator subunits identified and were shown to form a stable complex *in vivo*[12]. Subsequently, purification under milder conditions resulted in the identification of the second associated subcomplex containing subunits Elp4, Elp5 and Elp6 (refs. 13,14). Deletion of any of the six subunits in yeast, *Caenorhabditis elegans* or *Arabidopsis thaliana* leads to the loss of complex integrity, its dysfunction and almost identical *in vivo* phenotypes[7,15–17], emphasizing the importance of each individual subunit for Elongator function. In humans, Elongator appears primarily to affect the development and maintenance of the nervous system, as some individuals suffering from certain neurodegenerative diseases carry mutations or variants in one of the six human Elongator genes[18–20].

To deepen our mechanistic understanding of the evolutionarily conserved multisubunit Elongator complex and to better understand its role in multiple cellular processes, we solved the crystal structure of the *S. cerevisiae* Elp456 subcomplex at 2.1-Å resolution. Elp4, Elp5 and Elp6 adopted a RecA fold, forming a heterohexameric ring-like structure that resembles hexameric RecA-like ATPases. As with other hexameric ATPases, we found a specific interaction with nucleic acids, namely tRNA, and showed that an ATP-driven mechanism regulated the release of tRNA from Elp456. Finally, on the basis of results from size exclusion chromatography, *in vivo* interaction assays and negative-staining electron microscopy, we propose a model of how the Elp456 hexameric ring assembly is incorporated into the holo-Elongator complex. The crystal structure of the Elp456 subcomplex in combination with our complementary biochemical and *in vivo* analyses further supports a functional role of the Elongator complex in tRNA modification.

[1]European Molecular Biology Laboratory (EMBL), Structural and Computational Biology Unit, Heidelberg, Germany. [2]Equipe Labellisée La Ligue, Institut de Génétique et de Biologie Moléculaire et Cellulaire (IGBMC), Centre National de la Recherche Scientifique (CNRS) UMR7104, Inserm, U964, Illkirch, France. [3]Université de Strasbourg, Strasbourg, France. [4]Centre de Génétique Moléculaire, Gif sur Yvette, France. Correspondence should be addressed to B.S. (seraphin@igbmc.fr) or C.W.M. (cmueller@embl.de).

Received 7 June 2011; accepted 22 December 2011; published online 19 February 2012; doi:10.1038/nsmb.2234

RESULTS

The Elp456 subcomplex resembles a ring-shaped hexamer

To characterize the molecular details of the Elp456 subcomplex, we coexpressed *S. cerevisiae* Elp4, Elp5 and Elp6 (specifically, $Elp4_{66–426}$–$Elp5_{1–270}$–$Elp6_{6×His-1–273}$, forming a stable and well-expressed complex, hereafter referred to as rElp456) in *Escherichia coli*. After purification, a stoichiometric rElp456 subcomplex eluted from a gel filtration column at a volume consistent with a molecular weight of ~210 kDa, roughly twice the expected weight (**Supplementary Fig. 1**). This prompted us to investigate the overall shape of the complex by negative-staining electron microscopy, where we observed a homogenous sample of ring-shaped particles with pronounced central staining (**Fig. 1a**). Elp456 subcomplex containing full-length Elp4, Elp5 and Elp6 subunits, instead of the N- and C-terminally truncated versions in rElp456, eluted at the same volume and also formed ring-like particles with similar dimensions (data not shown). Processing of a selected set of rElp456 particles yielded different class averages, which clearly resembled a ring-shaped hexameric arrangement for rElp456 (**Fig. 1a** and **Supplementary Fig. 2**). To determine the number of Elp6 copies within the Elongator complex *in vivo*, we used a coprecipitation strategy using doubly tagged tandem affinity purification (TAP) and protein A (ProtA) or calmodulin-binding protein (CBP) and ProtA and control (ProtA-tagged) Elp yeast strains[21] (see Online Methods). As expected, the Elp1–5 proteins specifically coprecipitated with Elp6-ProtA (**Fig. 1b**, top). Notably, Elp6-CBP also coprecipitated Elp6-ProtA indicating the presence of at least two Elp6 subunits per fully assembled Elongator complex. Similar experiments with Elp4 and Elp5 (**Fig. 1b**, bottom) confirmed a stoichiometry of at least two for all Elp456 subcomplex components *in vivo*. From these results, we concluded that Elongator uses two copies of Elp4, Elp5 and Elp6 to build up a heterohexameric ring-shaped subcomplex *in vitro* and *in vivo*.

Crystal structure of the Elp456 subcomplex

To elucidate the details of hexamer assembly, we crystallized rElp456 and solved its structure at 2.1-Å resolution by the multiple-wavelength anomalous diffraction (MAD) method using selenomethionine (SeMet)-substituted protein (**Table 1**). The crystal structure confirmed that rElp456 formed a hexameric ring-like assembly, built up by alternating copies of Elp4, Elp5 and Elp6 (**Fig. 1c**). The pseudo–six-fold symmetry that we observed in our EM images was generated by the structural similarity among individual subunits. The cavity in the center of the hexameric ring had an asymmetric opening (~25 Å × 15 Å) and was crossed by two partially disordered loops reaching out from the two Elp5 subunits present in the complex. The overall architecture showed clear directionality and differences between the two faces of the ring (**Fig. 1d**). The two copies of Elp4, Elp5 and Elp6 related by noncrystallographic symmetry (NCS) were located opposite each other in the ring and did not differ considerably in conformation or position relative to neighboring subunits. Three different intersubunit interfaces were formed (870 $Å^2$ for Elp4-Elp5, 1,300 $Å^2$ for Elp4-Elp6 and 1,590 $Å^2$ for Elp5-Elp6), and the size and complexity of the contact areas between subunits Elp4, Elp5 and Elp6 found in the

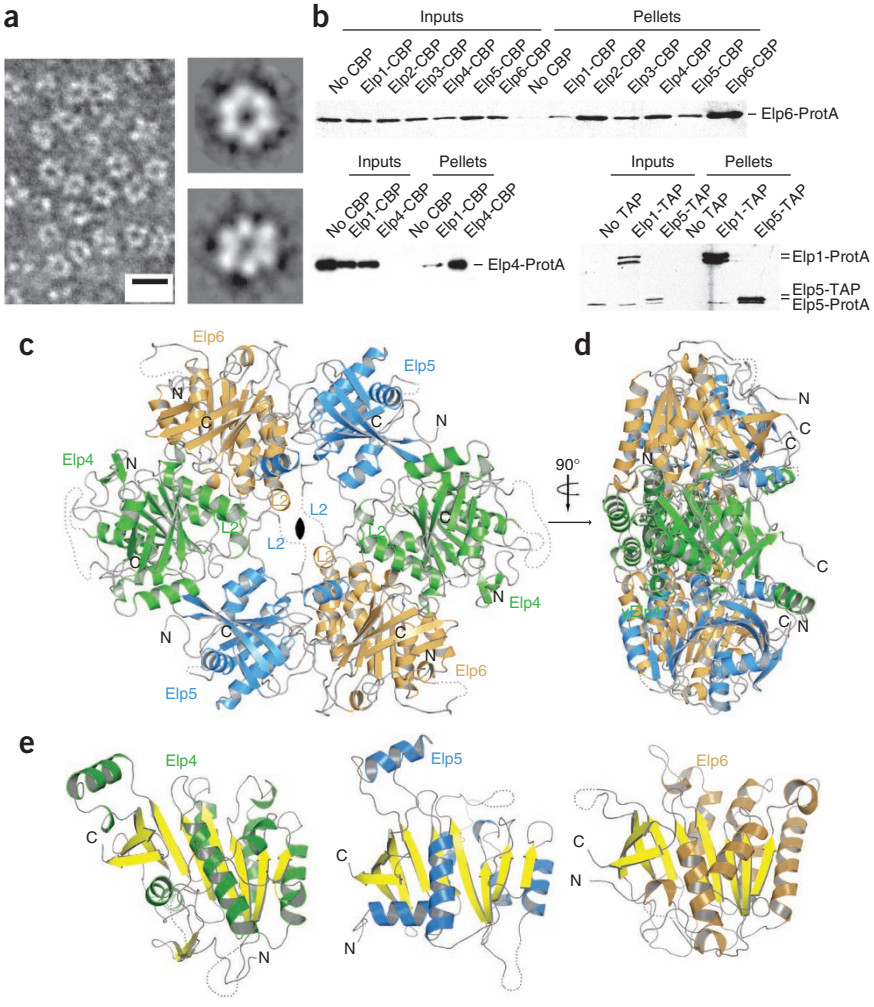

Figure 1 Hexameric structure of the rElp456 subcomplex. (**a**) Negative-staining electron microscopy and single particle analysis of rElp456. One raw image (left) and two representative class averages (right) are shown. Scale bar, 20 nm (left); box size, 64 × 64 pixels, corresponding to 217.6 Å × 217.6 Å (right). A complete set of the class averages obtained is shown in **Supplementary Figure 2**. (**b**) Western blot of SDS-PAGE separated CBP-tagged Elp proteins from yeast strains expressing Elp6-ProtA. Inputs correspond to total yeast extracts. Pellets show coprecipitated ProtA-tagged Elongator subunits. Chemiluminescence shows the presence of both subunits in a complex (note that the assay is not quantitative but only shows the presence of two differently tagged copies of the same subunit in the complex. Outer left "No CBP" lanes are input lanes; the other "No CBP" lanes show the background level). Similar experiments were conducted with Elp1-CBP, Elp4-CBP and control expressing Elp4-ProtA and with Elp1-TAP, Elp5-TAP and control expressing Elp5-ProtA (bottom panels). CBP, calmodulin-binding protein. (**c**) Crystal structure of the heterohexameric Elongator subcomplex rElp456. Dotted gray lines indicate disordered regions. The central dyad, L2 loops (named by analogy with RecA) and respective N and C termini are indicated. (**d**) Side view of rElp456. (**e**) Elp4, Elp5 and Elp6 have almost identical RecA folds. Individual subunits are oriented by their central β-sheets, which are highlighted in yellow, whereas peripheral structural elements are colored as in **c**.

Table 1 Data collection, phasing and refinement statistics

	Hi-res SeMet[a]	SeMet		
Data collection				
Space group	$P2_12_12_1$		$P2_12_12_1$	
Cell dimensions				
a, *b*, *c* (Å)	105.7,124.9,146.4		105.1,124.5,146.2	
		Peak	Inflection	Remote
Wavelength (Å)	0.9782	0.9792	0.9794	0.9753
Resolution (Å)	46.2–2.1 (2.2–2.1)	50–2.75 (2.9–2.75)	50–2.95 (3.11–2.95)	50–3.2 (3.37–3.2)
R_{merge}	0.131 (0.655)	0.119 (0.353)	0.127 (0.386)	0.122 (0.318)
$I / \sigma I$	7.3 (5.7)	4.2 (2.0)	4.3 (1.9)	4.7 (2.3)
Completeness (%)	98.8 (96.2)	100.0 (99.9)	100.0 (100.0)	100.0 (100.0)
Redundancy	5.8	4.6	4.6	4.7
Sites	32	32	32	32
Refinement				
Resolution (Å)	46.2–2.1			
No. reflections	111,986			
R_{work} / R_{free} (%)	20.0 / 23.1			
No. atoms	13,005			
Protein	12,143			
Water	862			
B-factors (Å^2)				
Protein	41.7			
Water	47.8			
R.m.s. deviations				
Bond lengths (Å)	0.01			
Bond angles (°)	1.158			

[a]Values for the highest-resolution shell are shown in parentheses. Hi-res, high-resolution.

ring-like arrangement was consistent with their stable association observed by size exclusion chromatography, electron microscopy and coprecipitation experiments (**Fig. 1a**,**b** and **Supplementary Fig. 1**). The dimensions of the rElp456 hexamer in our crystals (105 Å × 135 Å) were in good agreement with the size of the observed rElp456 EM particles (110–140 Å) (**Supplementary Fig. 2b**,**c**).

Elp4, Elp5 and Elp6 all adopted almost identical RecA folds, which consist of a central, mostly parallel, twisted β-sheet flanked by several α-helices (**Fig. 1e** and **Supplementary Fig. 3**). Whereas the RecA fold core comprises a five-stranded β-sheet[22], in Elp4, Elp5 and Elp6 this central β-sheet was extended by four additional strands. RecA-like ATPases belong to the additional strand catalytic glutamate (ASCE) superfamily of ring-translocases. Although different RecA-like ATPases have evolved individual characteristics serving their specific functions, many general features such as the RecA core, spatial arrangements of residues responsible for ATPase function, ability to bind specific nucleic acid substrates, nucleotide-dependent movement of substrate binding loops L1 and L2, and the homohexameric arrangement of subunits are found in most family members[22]. Models of the three Elongator subunits pairwise superimposed not only onto each other with r.m.s. deviations of ~2.85 Å but also to other RecA fold proteins including RecA[23], Rho[24] and the gene 4 protein (gp4) of T7 bacteriophage[25] (**Supplementary Fig. 3**). To our knowledge, the Elp456 subcomplex represents the first heterohexameric RecA-fold ATPase family member that establishes the typical hexameric ring-shape with three different proteins.

Elp456 specifically recognizes tRNA

RecA-like proteins are known to specifically bind, translocate and rearrange nucleic acids[22,26]. Therefore, we tested Elp456 *in vitro* for its affinity toward different radioactively labeled nucleic acids, namely single-stranded (ss) DNA, single-stranded oligo(U) RNA and tRNA. We observed a direct and specific interaction between yeast $tRNA_1^{Glu}$ and the rElp456 subcomplex ($K_{d,\ rElp456}$ = 1.2 ± 0.27 μM; $K_{d,\ Elp456\ full\text{-}length}$ = 1.4 ± 0.29 μM; **Fig. 2a** and **Supplementary Fig. 4**) but not with either oligo(U) RNA or ssDNA. The rElp56 dimer, which we used as a negative control, bound to none of the nucleic acids tested (**Fig. 2a**). In a competition experiment, an excess of unlabeled $tRNA_1^{Glu}$ anticodon loop displaced radioactively labeled $tRNA_1^{Glu}$ (**Fig. 2b**,**c**), suggesting that rElp456 recognizes tRNA through its anticodon loop. The mcm^5 and ncm^5 modifications affect 11 of the 13 yeast tRNAs with U at the wobble position[10], and overexpression of Lys-tRNA and Gln-tRNA genes rescues thermosensitive Elp mutants in yeast[6]; however, because most structural features of tRNAs are conserved and because $tRNA_1^{Glu}$ is known to interact with Elongator[7], we used $tRNA_1^{Glu}$ in our initial electrophoretic mobility shift assay (EMSA) experiments. To further explore whether Elp456 is able to discriminate between modifiable tRNAs carrying a uridine in the wobble base position, and non-modifiable anticodon loops, we mutated the wobble base position of $tRNA_1^{Glu}$ and tested the binding of these mutated tRNAs to rElp456. In addition, we tested $tRNA_2^{Glu}$, which has additional sequence variations outside the anticodon triplet and does not carry a modifiable wobble-base uridine, to identify other tRNA-specific recognition elements. As we did not observe any major differences in binding affinities of these different tested tRNAs (**Supplementary Fig. 4**), we speculate that Elongator mediates specificity for modifiable tRNAs not during binding to the Elp456 subcomplex but more likely during the modification reaction step itself.

Because hexameric ATPases interact with nucleic acid substrates through residues protruding from loops in the central cavity of the ring, we were curious as to whether similar interactions could be observed in Elp456 (refs. 24,27). We did not observe an extended, positively charged binding surface in the central cavity region of Elp456 that potentially could bind nucleic acids, whereas in the RecA-like Rho and T7gp4 hexamers more positively charged loop residues line the central pore (compare surface charges of the Elp456 subcomplex with those of the Rho and T7gp4 structures; **Supplementary Fig. 5**). The observed difference in surface charges correlates with the fact that the rElp456 subcomplex did not bind ssDNA or poly(U) RNA, but only tRNA. Next, we tested rElp456 subcomplexes bearing point mutations in the L2 loops of subunits Elp4, Elp5 and Elp6 (**Fig. 2d**) for their ability to bind to tRNA. Mutations of the most central L2 loop residues of Elp6 to alanine (V199A H200A) led to strongly lowered binding of tRNA to rElp456, but notably, they did not affect complex stability (**Supplementary Fig. 5**). Changing adjacent residues in the same loop by mutating residues 193–196 into alanines (Elp6 polyAla 193–196) or other areas did not affect tRNA binding (**Fig. 2e**). Consistent with these results, tRNA could be manually docked without steric clashes or major structural rearrangements to the Elp456 hexamer with the anticodon loop pointing into the central cavity (data not shown).

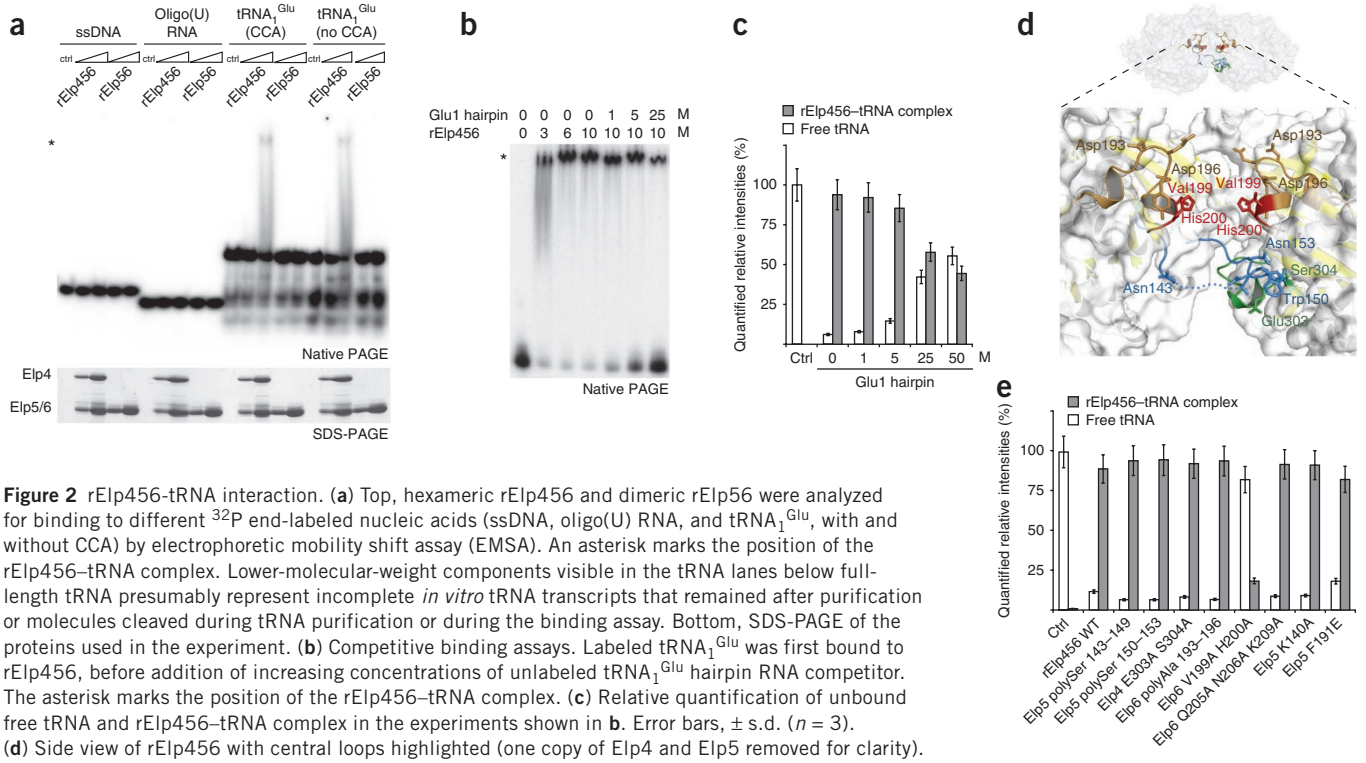

Figure 2 rElp456-tRNA interaction. (**a**) Top, hexameric rElp456 and dimeric rElp56 were analyzed for binding to different ^{32}P end-labeled nucleic acids (ssDNA, oligo(U) RNA, and $tRNA_1^{Glu}$, with and without CCA) by electrophoretic mobility shift assay (EMSA). An asterisk marks the position of the rElp456–tRNA complex. Lower-molecular-weight components visible in the tRNA lanes below full-length tRNA presumably represent incomplete *in vitro* tRNA transcripts that remained after purification or molecules cleaved during tRNA purification or during the binding assay. Bottom, SDS-PAGE of the proteins used in the experiment. (**b**) Competitive binding assays. Labeled $tRNA_1^{Glu}$ was first bound to rElp456, before addition of increasing concentrations of unlabeled $tRNA_1^{Glu}$ hairpin RNA competitor. The asterisk marks the position of the rElp456–tRNA complex. (**c**) Relative quantification of unbound free tRNA and rElp456–tRNA complex in the experiments shown in **b**. Error bars, ± s.d. ($n = 3$). (**d**) Side view of rElp456 with central loops highlighted (one copy of Elp4 and Elp5 removed for clarity). Mutated residues are shown in stick representation and are colored according to the respective subunit (Elp4 green, Elp5 blue, Elp6 brown). (**e**) EMSA analysis of rElp456–tRNA complex formation by mutated versions of rElp456 hexamers, carrying point mutations in the residues indicated in **d**. Relative quantification of unbound free tRNA and rElp456–tRNA complex formed. Error bars, ± s.d. ($n = 3$).

The Elp456 subcomplex is a hexameric ATPase

Despite the similarity to other RecA-fold proteins, Elp4, Elp5 and Elp6 lack the key sequence signature of ATPases, notably the Walker A motif (P-loop) (**Supplementary Fig. 6**). We nevertheless observe an intrinsic basal ATPase activity of the rElp456 subcomplex, whereas the rElp56 dimer possessed no substantial ATPase activity (**Fig. 3**). We observed similar hydrolysis rates for rElp456 and $Elp456_{full\text{-}length}$ (64.4 ± 6.0 and 54.9 ± 6.4 $\mu mol_{Pi\ released}\ mmol_{protein}^{-1}\ min^{-1}$, respectively; **Supplementary Table 1**) that are in the same range as basal ATPase activities for Rho and RecA determined by us

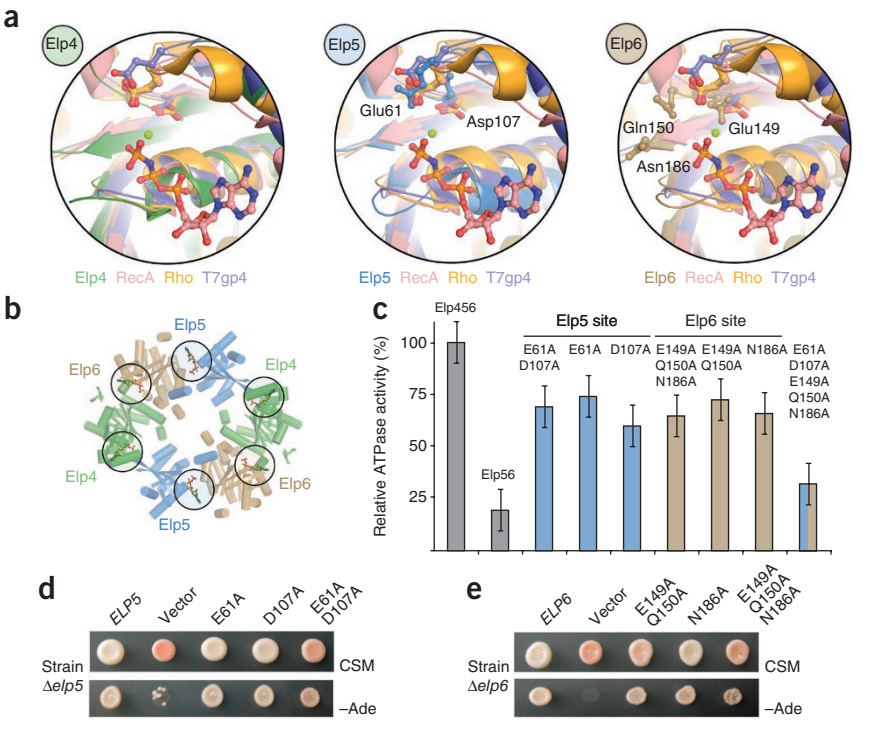

Figure 3 Elp456 is a hexameric ATPase. (**a**) Potential ATP binding sites in Elp4 (left), Elp5 (middle) and Elp6 (right). Crystal structures of Elp4 (green), Elp5 (blue) and Elp6 (brown) were superimposed on RecA (PDB 1XMS; salmon), Rho (PDB 3ICE, orange) and T7 gp4 (PDB 1E0K, violet). A bound AMP-PNP molecule (salmon, ball and stick) and Mg^{2+} (light green sphere) present in the RecA crystal structure (PDB 1XMS) illustrates nucleotide binding. Conserved and mutated residues are labeled and shown in stick representation. (**b**) Positions of potential ATP binding sites in the hexameric rElp456 subcomplex. AMP-PNP molecules from the RecA crystal structure (PDB 1XMS) superimposed onto Elp4, Elp5 and Elp6 are encircled. (**c**) ATPase activity assay of the intrinsic ATPase activity of wild-type rElp456 hexamer and mutated rElp456 hexamers carrying mutations in potential catalytic residues. Error bars, ± s.d. ($n = 3$). (**d**,**e**) Complementation of the *elp5* (**d**) or *elp6* (**e**) deletion strains (Δ*elp5* or Δ*elp6*) by various mutants. In the absence of Elp function (vector), cells are red on complete supplement medium (CSM) and do not grow on adenine-deficient CSM (–Ade). When Elongator is functional (wild type), cells are white on CSM and do grow on –Ade. Partial functions result in intermediate colors and growths.

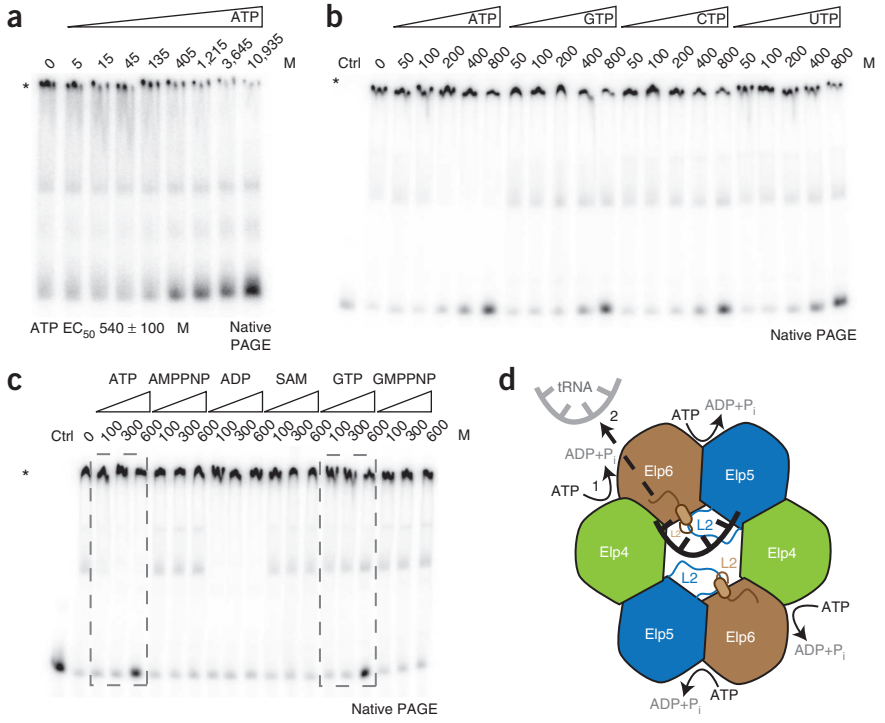

Figure 4 ATP regulates tRNA binding. (**a**) The electrophoretic mobility shift assay (EMSA) was used to monitor complex formation between hexameric rElp456 and tRNA in the presence of increasing amounts of ATP. (**b**) EMSA using increasing amounts of different nucleoside triphosphates (ATP, GTP, CTP and UTP). (**c**) EMSA using increasing amounts of hydrolyzable and non-hydrolyzable nucleotides. In **a**–**c**, an asterisk marks the position of the rElp456–tRNA complex. (**d**) Current working model of how ATP hydrolysis regulates tRNA binding and release.

(**Supplementary Table 1**) and others[28–30]. As in other RecA ATPases[31,32] we could not detect a nucleoside triphosphate specificity; the hydrolysis rates of rElp456 and $Elp456_{full\text{-}length}$ for UTP (72.7 ± 5.4 and 56.9 ± 3.7 $\mu mol_{Pi\ released}\ mmol_{protein}^{-1}\ min^{-1}$, respectively) were almost identical for ATP (**Supplementary Table 1**). Whereas the basal ATPase activities of Rho and RecA can be stimulated by their specific nucleic acid substrates (**Supplementary Table 1**), ATPase activity of the Elp456 subcomplex could not be stimulated by tRNA or the anticodon loop. This could correspond to an intrinsic difference between the Elp456 subcomplex and other hexameric RecA-like ATPases, but it could equally reflect the possibility that we have not yet identified the correct substrate intermediate or that other Elongator subunits Elp1, Elp2 and Elp3 contribute to stimulate the basal ATPase activity.

Mutating potential active site residues (**Fig. 3a**,**b**) within either Elp5 (E61, D107) or Elp6 (E149, Q150, N186) decreased the basal ATPase activity, an effect that was further enhanced by simultaneously mutating residues in both subunits (**Fig. 3c**). To exclude the possibility that the lowered ATPase activities of mutant protein containing Elp456 subcomplexes simply resulted from decreased complex stability, we used circular dichroism and native PAGE to confirm similar behavior of complexes containing wild-type and mutant proteins (**Supplementary Fig. 5**). Wild-type and mutant protein containing Elp456 subcomplexes showed similar melting temperatures (T_m of ~60 °C), well above the temperature (T = 30 °C) at which the ATPase assay was carried out. Furthermore, all complexes containing mutant proteins were stable and migrated similarly to the wild type on native PAGE gels, whereas monomeric Elp4 and the binary rElp56 complex showed higher electrophoretic mobilities. To further explore the role of Elongator in post-transcriptional tRNA modification, we tested the importance of these potential catalytic residues with an *in vivo* complementation assay that allowed the detection of mcm^5 modifications at the wobble position[7]. Whereas wild-type Elp5 and Elp6 were able to suppress the deletions of the cognate genes, mutant derivatives with compromised ATP hydrolysis activity only partly complemented these deletions (**Fig. 3d**). These data support a functional connection between ATP binding and hydrolysis activity of Elongator and its *in vivo* tRNA modification activity. The partial rescue of the Elp6 V199A H200A mutant in this *in vivo* complementation assay (data not shown) supported the likelihood of additional tRNA interaction sites in the context of the Elongator, a finding that is in agreement with other cross-linking experiments[7].

To further explore ATP-binding and ATPase activity of the Elp456 subcomplex, we tried to cocrystallize rElp456 with ATP, 5′-adenylyl imidodiphosphonate (AMP-PNP) and ATPγS. Unfortunately, no

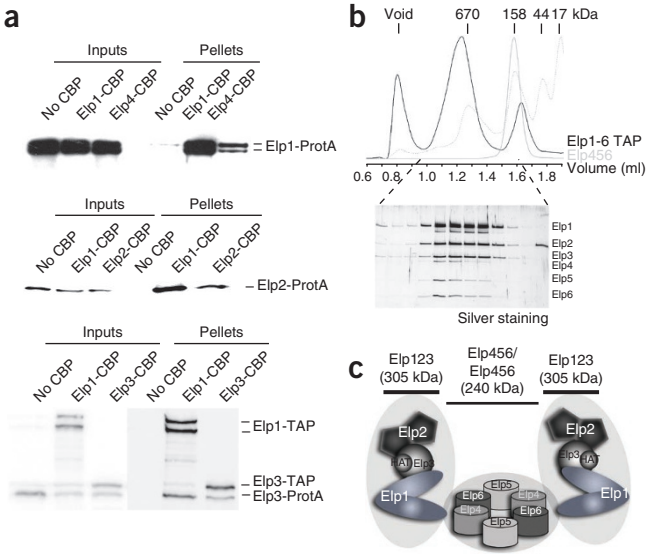

Figure 5 Integration of Elp456 subcomplex into the holo-Elongator complex. (**a**) Proteins in extracts from yeast strains expressing Elp1-ProtA with Elp1-CBP, Elp4-CBP, or a control expressing no CBP-tagged protein, were precipitated with calmodulin-coated beads and analyzed by western blot. Similar experiments were done with Elp1-CBP, Elp2-CBP and a control expressing Elp2-ProtA only, and with Elp1-TAP, Elp3-TAP and a control expressing Elp3-ProtA only. (**b**) UV (280 nm) absorption profiles of TAP-purified holo-Elongator complex, rElp456 subcomplex and molecular-weight markers on an analytical Superose 6 gel filtration column (3.1/30; upper panel). Holo-Elongator fractions were analyzed by SDS-PAGE followed by silver staining. (**c**) Schematic representation of the six-subunit holo-Elongator complex. Subunit compositions and estimated molecular weight of the respective subcomplexes are indicated.

crystals of the Elp456 subcomplex bound to nucleoside triphosphates or analogs were obtained. Soaking with the respective nucleotides notably decreased the diffraction quality of the crystals, but no nucleotides could be located in the data sets recorded so far.

ATPase activity of Elp456 regulates tRNA binding

Hexameric ATPases are known to use sophisticated communication mechanisms between their nucleic acid binding loops and their spatially separated ATP binding sites to translocate or rearrange nucleic acid substrates[24,26]. We wanted to investigate whether similar mechanisms were conserved in the heterohexameric arrangement of Elp456 by testing the influence of different hydrolyzable and non-hydrolyzable nucleotides on the observed rElp456-tRNA interaction. We observed a strong decrease in the affinity of the rElp456 subcomplex for tRNA in the presence of ATP (EC_{50} 540 ± 100 μM; **Fig. 4a**). The observed negative effect on tRNA binding was observed with other hydrolyzable nucleoside triphosphate (GTP, CTP and UTP; **Fig. 4b**). Notably, we did not observe this effect in presence of AMP-PNP, 5-guanylyl imidodiphosphate (GMP-PNP), ADP or *S*-adenosylmethionine (SAM) (**Fig. 4c**). These results exclude the possibility that ATP and tRNA simply compete for binding to the same basic patch on the surface of the Elp456 subcomplex. Rather, we concluded that ATP binding and subsequent hydrolysis of ATP either inhibited tRNA recruitment or promoted dissociation of tRNA from Elongator (**Fig. 4d**). We currently favor the second possibility, as it would allow the Elp456 subcomplex to orchestrate tRNA binding and ATPase activity in an ATP-dependent cycle similar to that observed for other RecA-like ATPases.

The Elp456 hexamer bridges two Elp123 subcomplexes

In contrast to other RecA-like ATPases, the Elp456 hexamer is part of a bigger macromolecular assembly. To understand how Elp456 is incorporated into the six-subunit Elongator complex, we extended the *in vivo* coimmunoprecipitation strategy described for Elp456 (**Fig. 1b**). As tagged Elp1, Elp2 and Elp3 were also able to specifically coprecipitate a second copy carrying a different tag (**Fig. 5a**), we concluded that there are at least two copies of each of the six subunits present in the holo-Elongator complex. Consistent with this stoichiometry, the molecular weight estimation (~850 kDa) using size exclusion chromatography of purified TAP-tagged holo-Elongator from yeast (**Fig. 5b**) indicated that the Elongator complex was a dodecamer containing two copies of each of the six Elongator subunits. Considering these results and the two-fold symmetry of Elp456, we propose a model in which one Elp456 hexamer bridges two peripherally attached Elp123 subcomplexes (**Fig. 5c**).

DISCUSSION

Mutations in genes that encode Elongator subunits lead to a large variety of molecular phenotypes. At present it is unclear whether this results from Elongator having different activities in various cellular processes or whether disruption of one defined molecular function of Elongator results in different phenotypic outcomes. In this study we presented the detailed structural and functional characterization of the *S. cerevisae* Elp456 subcomplex. Subunits Elp4, Elp5 and Elp6 share a RecA-like fold and assemble into a heterohexameric, ring-like structure. Our results provided a structure-based rationale for the importance of individual Elp4, Elp5 and Elp6 subunits for the functionality and integrity of the entire Elongator complex and suggested that the Elp456 heterohexamer bridges two peripherally attached Elp123 subcomplexes. In the context of the entire Elongator complex, we speculate that positioning the wobble base position of a tRNA directly above the central pore of the heterohexameric ring could explain the specificity of the modification reaction for wobble-base uridines by restricting their spatial accessibility. Furthermore, we showed that the Elp456 subcomplex specifically bound tRNA and that ATP inhibited the interaction with tRNA. Whereas other ring-shaped RecA-fold ATPases use energy derived from ATP hydrolysis to rearrange nucleic acids or translocate them through the central pore, the Elp456 subcomplex apparently uses ATP to control tRNA binding and release. The detailed mechanism that controls the interaction between the Elp456 subcomplex and tRNA is currently unknown. However, we favor a model in which ATP hydrolysis triggers the release of tRNA from Elongator, as it is most consistent with our data (**Fig. 4**). Alternatively, it is possible that ATP binding is sufficient to cause the release of tRNA and that the non-hydrolyzable ATP analogs AMP-PNP and GMP-PNP (**Fig. 4c**) do not mimic ATP faithfully enough to trigger tRNA dissociation. We are currently also investigating the connection between the tRNA modification reaction of Elongator and ATP recruitment, which might allow the precise temporal control of the modification reaction and subsequent tRNA release. It was an unexpected discovery that the Elp456 subcomplex is a heterohexameric RecA-like ATPase with many similarities to known homohexameric RecA-like translocases. Our results represent the first step toward a mechanistic understanding of Elongator function and further substantiate the role of Elongator in tRNA modification.

METHODS

Methods and any associated references are available in the online version of the paper at http://www.nature.com/nsmb/.

Accession codes. Protein Data Bank: Coordinates have been deposited with accession code 4A8J.

Note: Supplementary information is available on the Nature Structural & Molecular Biology website.

ACKNOWLEDGMENTS

The authors acknowledge support by the EMBL Proteomics Core Facility and the EMBL Heidelberg Crystallization Platform and access and support at the ESRF beamlines by the EMBL-ESRF Joint Structural Biology Group. We also thank F. Baudin, O. Barabas, C. Petosa, W. Hübner, C. Sachse and G. Male for comments on the manuscript; A.S. Byström (Umeå University) for the gift of yeast strains and plasmids; J.M. Berger (University of California, Berkeley) for recombinant *E. coli* Rho protein; D. Rentz, B. Bonneau and M. Correa for technical support; D. Lebert and V. Henriot for help in the early stages of this work; M. Argentini and D. Cornu (SICaPS, IMAGIF platform, Gif sur Yvette, France) for mass spectrometry analysis; and the Institut de Génétique et de Biologie Moléculaire et Cellulaire (IGBMC) for their assistance. This work was supported by the European Union 6th Framework programs '3D-Repertoire' (LSHG-CT-2005-512028) to C.W.M. and B.S.; and the CNRS and Ligue Contre le Cancer (Equipe Labellisée 2011) to B.S.

AUTHOR CONTRIBUTIONS

S.G. did the biochemical, biophysical and crystallographic analyses; J.L. optimized expression constructs and initial purifications; C.F. carried out coprecipitations, yeast assays and TAP purifications; N.M.I.T. did the electron microscopy analysis; and S.G., B.S. and C.W.M. designed experiments, analyzed the data and wrote the manuscript.

COMPETING FINANCIAL INTERESTS

The authors declare no competing financial interests.

Published online at http://www.nature.com/nsmb/.
Reprints and permissions information is available online at http://www.nature.com/reprints/index.html.

1. Wittschieben, B.O. *et al.* A novel histone acetyltransferase is an integral subunit of elongating RNA polymerase II holoenzyme. *Mol. Cell* **4**, 123–128 (1999).
2. Rahl, P.B., Chen, C.Z. & Collins, R.N. Elp1p, the yeast homolog of the FD disease syndrome protein, negatively regulates exocytosis independently of transcriptional elongation. *Mol. Cell* **17**, 841–853 (2005).

3. Creppe, C. *et al.* Elongator controls the migration and differentiation of cortical neurons through acetylation of α-tubulin. *Cell* **136**, 551–564 (2009).
4. Li, Q. *et al.* The Elongator complex interacts with PCNA and modulates transcriptional silencing and sensitivity to DNA damage agents. *PLoS Genet.* **5**, e1000684 (2009).
5. Okada, Y., Yamagata, K., Hong, K., Wakayama, T. & Zhang, Y. A role for the Elongator complex in zygotic paternal genome demethylation. *Nature* **463**, 554–558 (2010).
6. Esberg, A., Huang, B., Johansson, M.J.O. & Bystrom, A.S. Elevated levels of two tRNA species bypass the requirement for elongator complex in transcription and exocytosis. *Mol. Cell* **24**, 139–148 (2006).
7. Huang, B., Johansson, M.J.O. & Bystrom, A.S. An early step in wobble uridine tRNA modification requires the Elongator complex. *RNA* **11**, 424–436 (2005).
8. Grosjean, H., de Crecy-Lagard, V. & Marck, C. Deciphering synonymous codons in the three domains of life: co-evolution with specific tRNA modification enzymes. *FEBS Lett.* **584**, 252–264 (2010).
9. Huang, B., Lu, J. & Bystrom, A.S. A genome-wide screen identifies genes required for formation of the wobble nucleoside 5-methoxycarbonylmethyl-2-thiouridine in *Saccharomyces cerevisiae*. *RNA* **14**, 2183–2194 (2008).
10. Johansson, M.J.O., Esberg, A., Huang, B., Bjork, G.R. & Bystrom, A.S. Eukaryotic wobble uridine modifications promote a functionally redundant decoding system. *Mol. Cell. Biol.* **28**, 3301–3312 (2008).
11. Murphy, F.V.t., Ramakrishnan, V., Malkiewicz, A. & Agris, P.F. The role of modifications in codon discrimination by $tRNA^{Lys}_{UUU}$. *Nat. Struct. Mol. Biol.* **11**, 1186–1191 (2004).
12. Otero, G. *et al.* Elongator, a multisubunit component of a novel RNA polymerase II holoenzyme for transcriptional elongation. *Mol. Cell* **3**, 109–118 (1999).
13. Krogan, N.J. & Greenblatt, J.F. Characterization of a six-subunit holo-elongator complex required for the regulated expression of a group of genes in *Saccharomyces cerevisiae*. *Mol. Cell. Biol.* **21**, 8203–8212 (2001).
14. Winkler, G.S. *et al.* RNA polymerase II elongator holoenzyme is composed of two discrete subcomplexes. *J. Biol. Chem.* **276**, 32743–32749 (2001).
15. Frohloff, F., Fichtner, L., Jablonowski, D., Breunig, K.D. & Schaffrath, R. *Saccharomyces cerevisiae* Elongator mutations confer resistance to the *Kluyveromyces lactis* zymocin. *EMBO J.* **20**, 1993–2003 (2001).
16. Mehlgarten, C. *et al.* Elongator function in tRNA wobble uridine modification is conserved between yeast and plants. *Mol. Microbiol.* **76**, 1082–1094 (2010).
17. Chen, C., Tuck, S. & Bystrom, A.S. Defects in tRNA modification associated with neurological and developmental dysfunctions in *Caenorhabditis elegans* Elongator mutants. *PLoS Genet.* **5**, e1000561 (2009).
18. Anderson, S.L. *et al.* Familial dysautonomia is caused by mutations of the *IKAP* gene. *Am. J. Hum. Genet.* **68**, 753–758 (2001).
19. Simpson, C.L. *et al.* Variants of the elongator protein 3 (ELP3) gene are associated with motor neuron degeneration. *Hum. Mol. Genet.* **18**, 472–481 (2009).
20. Strug, L.J. *et al.* Centrotemporal sharp wave EEG trait in rolandic epilepsy maps to Elongator protein complex 4 (ELP4). *Eur. J. Hum. Genet.* **17**, 1171–1181 (2009).
21. Salgado-Garrido, J., Bragado-Nilsson, E., Kandels-Lewis, S. & Seraphin, B. Sm and Sm-like proteins assemble in two related complexes of deep evolutionary origin. *EMBO J.* **18**, 3451–3462 (1999).
22. Lyubimov, A.Y., Strycharska, M. & Berger, J.M. The nuts and bolts of ring-translocase structure and mechanism. *Curr. Opin. Struct. Biol.* **21**, 240–248 (2011).
23. Story, R.M., Weber, I.T. & Steitz, T.A. The structure of the *Escherichia coli* RecA protein monomer and polymer. *Nature* **355**, 318–325 (1992).
24. Thomsen, N.D. & Berger, J.M. Running in reverse: the structural basis for translocation polarity in hexameric helicases. *Cell* **139**, 523–534 (2009).
25. Singleton, M.R., Sawaya, M.R., Ellenberger, T. & Wigley, D.B. Crystal structure of T7 gene 4 ring helicase indicates a mechanism for sequential hydrolysis of nucleotides. *Cell* **101**, 589–600 (2000).
26. Singleton, M.R., Dillingham, M.S. & Wigley, D.B. Structure and mechanism of helicases and nucleic acid translocases. *Annu. Rev. Biochem.* **76**, 23–50 (2007).
27. Enemark, E.J. & Joshua-Tor, L. Mechanism of DNA translocation in a replicative hexameric helicase. *Nature* **442**, 270–275 (2006).
28. Brenner, S.L. *et al.* RecA protein-promoted ATP hydrolysis occurs throughout RecA nucleoprotein filaments. *J. Biol. Chem.* **262**, 4011–4016 (1987).
29. Weinstock, G.M., McEntee, K. & Lehman, I.R. Hydrolysis of nucleoside triphosphates catalyzed by the RecA protein of *Escherichia coli*. Characterization of ATP hydrolysis. *J. Biol. Chem.* **256**, 8829–8834 (1981).
30. Richardson, J.P. & Carey, J.L. III. rho Factors from polarity suppressor mutants with defects in their RNA interactions. *J. Biol. Chem.* **257**, 5767–5771 (1982).
31. Weinstock, G.M., McEntee, K. & Lehman, I.R. Hydrolysis of nucleoside triphosphates catalyzed by the RecA protein of *Escherichia coli*. Hydrolysis of UTP. *J. Biol. Chem.* **256**, 8856–8858 (1981).
32. Lowery, C. & Richardson, J.P. Characterization of the nucleoside triphosphate phosphohydrolase (ATPase) activity of RNA synthesis termination factor p. I. Enzymatic properties and effects of inhibitors. *J. Biol. Chem.* **252**, 1375–1380 (1977).

ONLINE METHODS

Plasmids and strains. Yeast strains and plasmids are listed and described in detail in the **Supplementary Methods**.

Expression and purification of rElp456. An iterative trial-and-error process starting from constructs that encode different combinations of full-length Elp4, Elp5 and Elp6, including a single 6×His-tagged protein, was used, in combination with mass spectrometry analyses, to define stable, interacting and well-expressed protein constructs. This yielded the final construct, pBS3576, that encodes 6×His-$Elp6_{1–273}$, $Elp5_{1–270}$, $Elp4_{66–426}$ placed in this order for coexpression using a pET24d derived vector. Native and selenomethionine substituted protein complexes were expressed in *E. coli* (BL21 Gold (DE3); 18 °C overnight for 12–15 h). Bacteria cells were lysed using a French press in 50 mM Tris-HCl (pH 7.5), 300 mM NaCl, 10 mM imidazole, 1 mM DTT, 5% (v/v) glycerol and protease inhibitors. The soluble fraction was cleared by centrifugation (20,000*g* for 45 min at 4 °C), and 6×His-tagged complexes were purified with NiNTA affinity chromatography, followed by gel filtration with a Superdex 200 column (GE Healthcare) in 20 mM Tris-HCl (pH 7.5), 150 mM NaCl, 5 mM DTT and 1 mM $MgCl_2$.

Negative-staining electron microscopy. EM sample preparation, EM data collection and processing procedures are described in the **Supplementary Methods**.

Coimmunoprecipitation assays. Small-scale protein extracts[33] were prepared from yeast strains doubly tagged for two Elp proteins (with TAP and ProtA or CBP and ProtA), and a control strain with one Elp protein tagged with ProtA, which were used for precipitation with calmodulin-coated beads[21]. Proteins eluted from the beads with EGTA were separated by SDS-PAGE and analyzed by western blotting with PAP complex (Sigma) and chemiluminescence detection.

Crystallization and X-ray structure determination. Crystals were obtained by the hanging-drop vapor diffusion method after 3–7 d at 18 °C with 200 mM $MgCl_2$, 100 mM Tris-HCl (pH 7.5) and 25% (w/v) polyethylene glycol monomethyl ether 2,000 (PEG 2K MME) as precipitant. Crystals were cryoprotected by soaking them in reservoir solution supplemented with 15% (v/v) glycerol and flash cooled in liquid nitrogen at 100 K. Native and selenomethionine data were collected at ESRF beamlines ID23-2 and ID23-1 on MarMOSAIC and ADSC Q315 CCD detectors, respectively. The space group was determined to be $P2_12_12_1$ (a = 105.1 Å, b = 124.5 Å, c = 146.2 Å) with two molecules per asymmetric unit. Data processing was done with XDS[34] and programs of the CCP4 suite[35]. Thirty-two out of 40 possible selenium sites were initially located, and MAD phases were calculated from these positions using autoSHARP[36]. The obtained phase information was further improved using NCS averaging and solvent flattening with the program DM[35]. The resulting electron density map was of good quality, and selenium sites were used for sequence assignment to build an initial model. This model was refined against a high resolution SeMet data set using Phenix[37] to a final model with R_{work}/R_{free} of 20.2/24.4% at 2.1-Å resolution (**Table 1**) and excellent geometry with 0% outliers, 3.9% in allowed regions, 96.1% in preferred regions of the Ramachandran plot, according to Molprobity[38]. Model figures and superimpositions were prepared using programs PyMOL (DeLano Scientific) and Coot[39].

Radioactive EMSA gel assays. Nucleic acids were labeled with 32P by T4 PNK[40] and gel purified on denaturing 15% (w/v) urea-PAGE. Radioactively labeled ^{32}P tRNA was first renatured by heating in water at 95 °C for 1 min, cooled down to 25 °C and incubated in 20 mM Tris-HCl (pH 7.5), 150 mM NaCl, 1 mM DTT, 1 mM $MgCl_2$ and 10 units RNasin (Promega). To quantify binding of rElp456 and $Elp456_{full\text{-}length}$ to $tRNA_1^{Glu}$, proteins were serially diluted from 12.8 µM to 0.1 µM in a final volume of 18 µl, followed by addition of 2 µl of renatured ^{32}P-labeled RNA (~5,000 cpm). After incubation at 28 °C for 30 min, the reactions were loaded on a 15% (w/v) native gel. For each experiment, a blank reaction was done. Because the amount of labeled tRNA is negligibly low (estimated concentration of 0.1–0.01 nM), an apparent K_d can be estimated from the protein concentration at 50% tRNA binding. Binding experiments using radioactively labeled ssDNA, oligo(U) RNA, $tRNA_1^{Glu}$ and $tRNA_1^{Glu}$ without CCA were carried out with 0.1 µM and 1 µM of rElp456 and rElp56 proteins. For competition experiments, ^{32}P-labeled $tRNA_1^{Glu}$ was first bound to 10 µM proteins, and then increasing concentrations of unlabeled competitor Glu1 hairpin (1–25 µM) were used to challenge the complex.

ATP hydrolysis assay. Purified rElp456 and indicated mutant proteins were additionally purified using hydrophobicity affinity chromatography (Source 15Phe, GE Healthcare) and analyzed for the absence of contaminating chaperones by SDS-PAGE followed by silver staining. Rho protein (kind gift of J. Berger) and RecA (New England Biolabs) were re-purified by gel filtration (Superdex 200, GE Healthcare). The assay buffer contained 75 mM Tris-HCl pH 7.5, 100 mM NaCl, 2.5 mM $MgCl_2$, 1 mM ATP. ATP hydrolysis rates were determined using the PiColorLock Gold Assay kit (Innova Biosciences, UK) according to the manufacturer's instructions.

***In vivo* complementation assays.** Complementing plasmids that encode wild-type ELP4 (pABY1518) or ELP6 (pABY1512) in the pRS315 vector were obtained from A.S. Byström[7]. A complementing plasmid that encodes wild-type ELP5, pBS3942 was constructed. Most of the mutant derivatives were obtained by inserting in the cognate vectors three PCR fragments covering roughly the promoter region, coding sequence and terminator region using the Cold Fusion strategy (System BioSciences). For point mutants the resulting plasmids were generated: pBS3987 (Elp5 E181A), pBS3988 (Elp5 D107A), pBS3990 (Elp5 E181A D107A), pBS3992 (Elp6 E149A Q150A N186A), pBS4036 (Elp6 E149A Q150A) and pBS4037 (Elp6 N186A). Because of polymorphism between the clone used to express the recombinant Elp6 and the complementing plasmid, we also generated a cognate control wild type pBS3991 (WT ELP6 variant) that behaved identically to plasmid pABY1512.

holo-Elongator TAP tagging and purification. To purify the holo-Elongator complex, a cassette that encodes the TAP tag and a TRP1 selection marker[41] was inserted downstream and in frame with ELP1 in strain BMA64 giving BSY2367. TAP purifications were done as previously described[42]. The holo-Elongator complex was further analyzed on a Superose 6 gel filtration column (GE Healthcare).

33. Séraphin, B. Sm and Sm-like proteins belong to a large family: identification of proteins of the U6 as well as the U1, U2, U4 and U5 snRNPs. *EMBO J.* **14**, 2089–2098 (1995).
34. Kabsch, W. Xds. *Acta Crystallogr. D Biol. Crystallogr.* **66**, 125–132 (2010).
35. CCP4. The Ccp4 suite—programs for protein crystallography. *Acta Crystallogr. D Biol. Crystallogr.* **50**, 760–763 (1994).
36. delaFortelle, E. & Bricogne, G. Maximum-likelihood heavy-atom parameter refinement for multiple isomorphous replacement and multiwavelength anomalous diffraction methods. *Methods Enzymol.* **276**, 472–494 (1997).
37. Adams, P.D. *et al.* PHENIX: building new software for automated crystallographic structure determination. *Acta Crystallogr. D Biol. Crystallogr.* **58**, 1948–1954 (2002).
38. Davis, I.W. *et al.* MolProbity: all-atom contacts and structure validation for proteins and nucleic acids. *Nucleic Acids Res.* **35**, W375–W383 (2007).
39. Emsley, P. & Cowtan, K. Coot: model-building tools for molecular graphics. *Acta Crystallogr. D Biol. Crystallogr.* **60**, 2126–2132 (2004).
40. Baudin, F., Bach, C., Cusack, S. & Ruigrok, R.W. Structure of influenza virus RNP. I. Influenza virus nucleoprotein melts secondary structure in panhandle RNA and exposes the bases to the solvent. *EMBO J.* **13**, 3158–3165 (1994).
41. Puig, O. *et al.* The tandem affinity purification (TAP) method: a general procedure of protein complex purification. *Methods* **24**, 218–229 (2001).
42. Rigaut, G. *et al.* A generic protein purification method for protein complex characterization and proteome exploration. *Nat. Biotechnol.* **17**, 1030–1032 (1999).